https://doi.org/10.1016/j.ijmecsci.2018.10.057

Tool interference at workpiece centre in single-point diamond turning

Guoqing Zhang[a], Yuqi Dai[a], Suet To[b], Xiaoyu Wu[a,*], Yan Lou[a]

[a]Guangdong Provincial Key Laboratory of Micro/Nano Optomechatronics Engineering, College of Mechatronics and Control Engineering, Shenzhen University, Nan-hai Ave 3688, Shenzhen 518060, Guangdong, PR China

[b]State Key Laboratory of Ultra-precision Machining Technology, Department of Industrial and Systems Engineering, The Hong Kong Polytechnic University, Kowloon, Hong Kong, PR China

* Corresponding Author / E-mail: wuxy@szu.edu.cn, Tel: +86-755-22673853, Fax: +86- 755-26557471

Abstract: In single-point diamond turning (SPDT), the workpiece centre error owing to the tool height below or above the spindle axis causes cylinder or cone appearances at the workpiece centre. The formed cone or cylinder boundary is used to identify the tool height and then compensate for it, in order to obtain the desired surface profile. As opposed to previous studies, based on the fact that the diamond tool is elevated during cone formation and therefore forms a tool interference zone with higher land and larger radius, this research conducts a theoretical and experimental study to investigate the origin of tool interference owing to centre error, and its influencing factors. In this study, the relation between centre error and interference force was investigated. A series of experiments were conducted to explore tool interference generation and its influencing factors. A mathematical model was derived to calculate the tool interference zone radius, whereby the relation between this radius and the cutting conditions was established. Moreover, the error sources between the theoretical and experimental results were analysed. As centre error can only be reduced by compensation and cannot be eliminated, particularly in machine tools with poor resolution, it is meaningful to conduct research on the centre cone generation and its influence on tool interference in SPDT, as well as suppressing the tool interference in SPDT. Furthermore, this research provides a reference for establishing an online force-based centre error identification method, thereby improving cutting efficiency.

Keywords: centre error; single-point diamond turning; tool interference; centre cone

1. Introduction

Single-point diamond turning (SPDT) is a turning process in which a single crystal diamond is employed as the cutting tool. According to Evans et al. (1987) and Hao et al. (2014), a natural diamond provides nano metric edge sharpness and effective wear resistance, and can cut ultra-high quality surfaces [1, 2]. SPDT has been an essential method to fabricate rotational-symmetric optical products with nano metric surface finish and sub-micron form accuracy, and therefore be widely used in fields such as lasers [3], optics [4], aerospace, military equipment [5], and communications. As the topography and roughness of a machined surface directly affects the product functions, studying the surface generation and machining error in SPDT is a significant topic. To date, surface generation in SPDT has been fully investigated in both experiment-based [6, 7] and model-based [8, 9] analyses. Experiment-based methods mainly analyse the measurement data obtained from stylus-type and optical interferometric instruments, which is inadequate for understanding the fundamentals of SPDT surface generation. Model-based analysis can fully reveal the tool-workpiece cutting kinematics during SPDT; therefore, it is beneficial for understanding the surface generation mechanism. However, model-based analysis fails to present occasional factors and their effects on SPDT surface generation.

Error sources and their effects on the machined surface finish have been extensively investigated [10, 11]. Juergens et al. (2003) categorised the SPDT error sources into tool decentre error, slide tilt error, thermal effects, spindle vibration, mounting stress and centripetal distortion [12]. Tool decentre occurs when the cutting tool is horizontally misaligned with the spindle axis, and includes ‘tool not to centre’ and ‘tool past centre’, where ‘tool not to centre’ will produce an M-shaped form error, while ‘tool past centre’ will result in a W-shaped form error [13]. Tool decentre will deform the machined surface profile and affect its form accuracy. Slide error will distort the cutting tool feed route in both the direction of normal to the surface and along the surface, thereby causing a

rotational symmetric surface wave [14, 15]. Thermal effect is a key factor affecting machining accuracy, and according to Bryan (1990), errors induced by the thermal effect may account for approximately 40%−70% of the total error budget [16]. The thermal effect can deform the relative position between the cutting tool and workpiece, eventually leading to machining errors [17, 18]. Spindle vibration owing to poor work spindle stiffness, unbalanced workpiece mounting and the air-hammer effect will cause three forms of high-frequency spindle motion: axial, radial and tilting motion [19, 20]. Multimode spindle vibration will result in the formation of a 'spindle star' on the machined surface, which affects the form accuracy [21, 22]. Tool tip vibration also has certain effects on the surface finish in SPDT, and tool tip vibration in SPDT will generally result in characteristic marks with small amplitudes and high frequencies [23, 24]. In addition to the above factors, mounting stress error and centripetal distortion are significant factors affecting the machined surface form accuracy in SPDT. These errors are known as mounting-caused errors, which can be suppressed by improving the workpiece mounting method; for example, by adopting a vacuum chuck to suppress the mounting stress, or balancing the workpiece to reduce centripetal distortion.

Centre error in SPDT is another key factor affecting the machined surface finish. It has been established that centre error owing to a tool height below the spindle axis will cause a cylinder appearance at the machined surface centre, as is shown in Fig. 1 (a), while a tool height above the spindle axis will lead to a cone appearance (see Fig. 1 (b)) [13]. The formed cone or cylinder boundary is used to identify the tool height and then compensate for it in order to obtain the desired surface profile. However, the cone or cylinder boundary measurement requires the workpiece to be dismounted first, and mounted again following measurement. This process also necessitates tool setting and balancing work; therefore, it is time consuming and will disturb the cutting continuity. Moreover, although a conventional method can be used to compensate for the centre error by measuring the bottom radius of the centre cone or cylinder, this can only reduce the centre error, and cannot eliminate it, particularly in machine tools with poor resolution. Therefore, an effective online centre error identification and suppression method is required that can identify the centre error online and compensate for it by adjusting the tool height. It was determined from our experiment that a tool interference zone with a larger radius is formed around the centre cone as opposed to the centre cylinder, which is proven to be formed by tool interference. Furthermore, our research confirmed that tool interference occurs when the tool height is above the spindle axis, as tool elevation has a threshold, and a smaller centre error may not cause obvious tool elevation; therefore, the tool interference zone may not be easily observed. According to Cheung and Lee (2002), tool interference in SPDT will change the tool kinematics and affect the surface finish [25]. Therefore, the tool interference zone caused by tool interference will affect both the form accuracy and roughness of the machined surface, and further affects the machined product function. Therefore, it is meaningful to conduct research to reveal the tool interference mechanism and tool interference zone suppression by adjusting the cutting parameters.

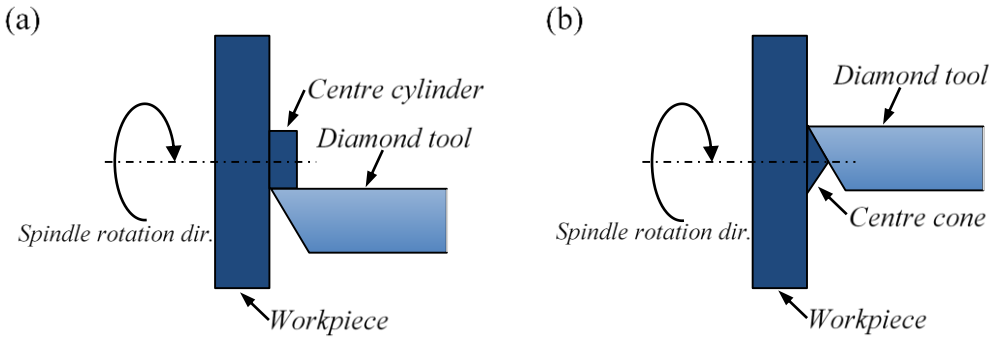

Fig. 1 Schematic diagram of (a) centre cylinder and (b) centre cone formation

In this study, tool interference generation owing to centre error was investigated, and influencing factors of the tool interference zone were explored. A mathematical model was established to calculate the tool interference zone

radius, based on which the effects of the centre error, cut depth, tool nose radius and tool clearance angle on the tool interference zone radius were studied. This research provides a fundamental understanding of the centre cone generation and induced tool interference, which may be used to predict the centre error and suppress the effects thereof on tool interference.

2. Experiments

In this research, a series of flat face turning were performed on an Optoform 30 two-axis CNC ultra-precision machine. The experimental setup is illustrated in Fig. 2 (a), diamond cutting tool was used in the present research, whose geometry is described by several parameters as shown in Fig 2 (b). During the turning, the workpiece was held on the spindle by a chuck, while the diamond tool was mounted on a height-adjustable tool holder, the diamond tool moves along the X direction of the machine tool to give a feed, while spindle carrying workpiece rotates to give a main cutting movement, the relative motion between cutting tool and workpiece removes workpiece material to realize the face turning. In the present research, each face turning operation was performed by 10 passes. In order to capture the cutting force, a three-channel Kistler 9252A force dynamometer was mounted between the diamond tool and tool holder, the force component directions are indicated in Fig. 2(c). The captured cutting force signal was then transferred to the post-processing software for analysis and to identify the useful information.

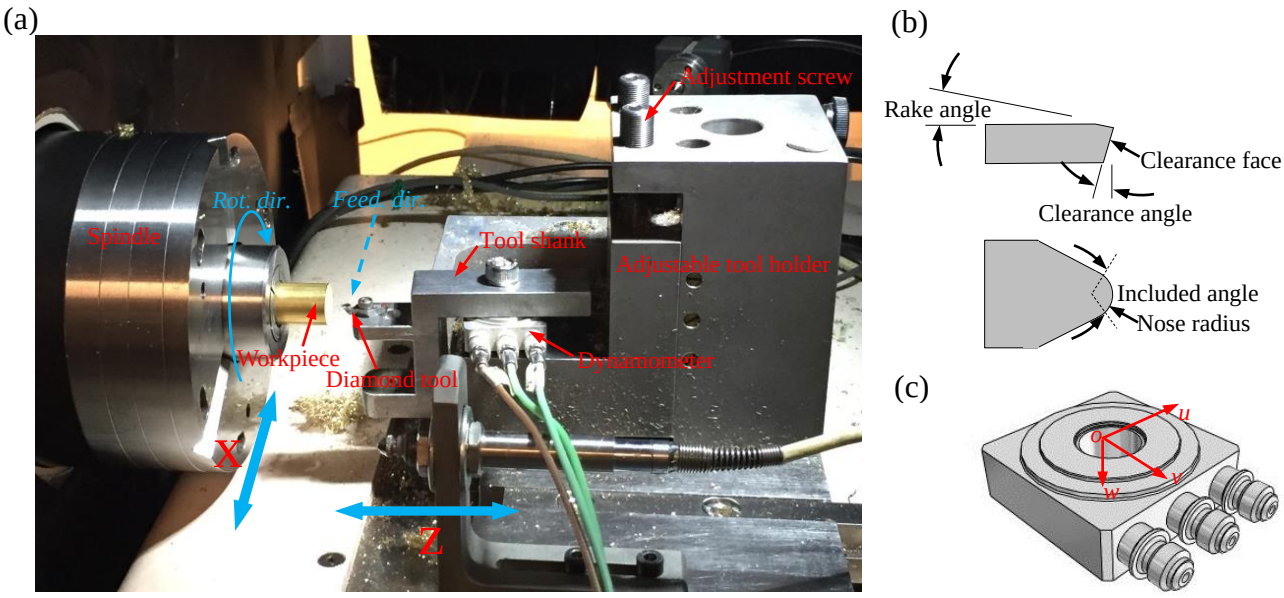

Fig. 2 (a) Experimental setup, (b) geometric parameters of diamond tools and (c) force component directions of the dynamometer (Kistler 9252A)

In this study, the centre error was first obtained by means offline optical microscope measurement, and then adjusted by the tool holder adjusting screw, under the guidance of a Mitutoyo dial gauge (513-304GE). During the adjustment process, the dial gauge contacted the tool holder; therefore, the adjustment could be monitored. The Mitutoyo dial gauge (513-304GE) has a submicron resolution, so the tool centre error could be adjusted to the desired valued.

In this research, brass was used as the workpiece material. The cutting parameters used in the experiment are listed in Table 1. The cutting experiment was performed under four conditions: cutting condition 1 was used to explore the effects of the cutting parameters on the tool interference zone; cutting conditions 2 and 3 were used to compare the effects of the tool nose radius on the tool interference zone; and cutting conditions 3 and 4 were used to compare the effects of the tool clearance angle on the tool interference zone. Following cutting, the machined

surface was measured by an optical microscope (Leica DM 2700M) and white light interferometer (Wyko NT 8000).

Table 1.

Cutting conditions used in experiment.

Parameters	Condition 1	Condition 2	Condition 3	Condition 4
Tool type	Single-crystal diamond tool	Single-crystal diamond tool	Single-crystal diamond tool	Single-crystal diamond tool
Rake angle	0 °	0 °	0 °	0 °
Clearance angle (δ)	10 °	15 °	15 °	5 °
Tool radius (R)	0.281 mm	0.101 mm	0.514 mm	0.493 mm
Feed rate (F_r)	5、(10)、50 mm/min	5 mm/min	5 mm/min	5 mm/min
Spindle speed (S_p)	(2000)、4000、6000 rpm	2000 rpm	2000 rpm	2000 rpm
Cut depth (a_p)	5、(10)、20 μm	8 μm	8 μm	8 μm
Passes	10	10	10	10

3. Results and discussion

3.1 Tool interference origin identification

In SPDT, it is well known that a tool height below the spindle axis will cause a cylinder appearance at the machined surface centre (as illustrated in Fig. 3 (a)), while a tool height above the spindle axis will lead to a cone appearance at the machined surface centre (as illustrated in Fig. 3 (c)). It can be observed from Fig. 3 that, when the centre cone is formed, a round highland is generated around the cone, with a larger radius and higher land, as indicated in Fig. 3 (c), which is not found in the centre cylinder formation (see Fig. 3 (a)). The round highland formation can also be reflected by the captured cutting force. It is found that the cutting force exhibits a sharp rise and decline at the end of the turning process when the tool height is above the spindle axis, performing a force pulse, as indicated in Fig. 3 (d), which differs significantly from the cutting force forms when the tool height is below the spindle axis, as illustrated in Fig. 3 (b). As the force pulse and round highland formation occur almost simultaneously, the force pulse located at the end of the turning process is believed to be related to the round highland formation.

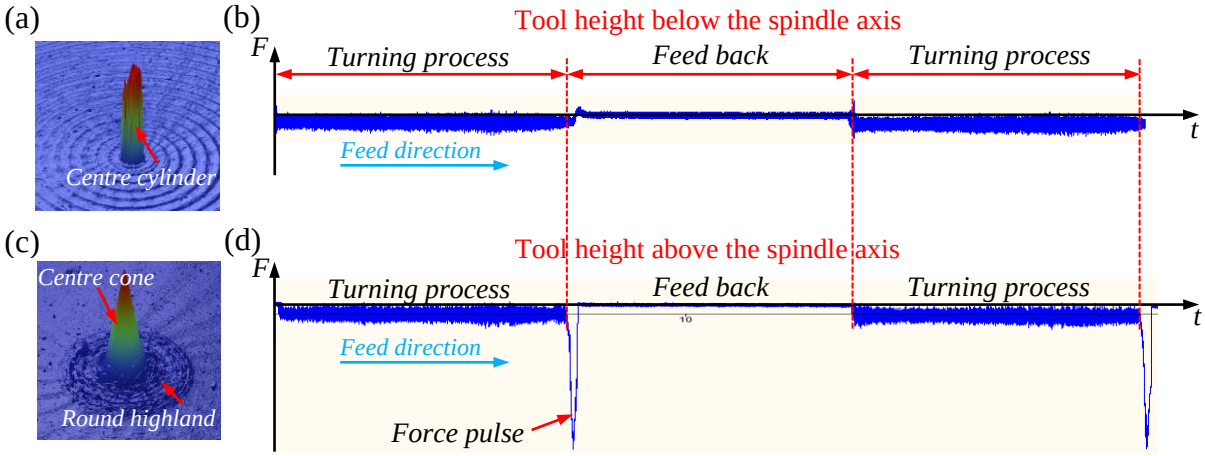

Fig. 3 Centre cylinder and cone appearances and corresponding cutting force forms (cutting parameters: S_p=2000 rpm, a_p=10 μm, F_r=10 mm/min, R=0.281 mm, δ=10 °)

Figure 4 illustrates the 3D display and its sectional profiles for both the centre cylinder and centre cone. Figure 4 (a) reveals that the side lines of both the centre cylinder X and Y profiles are a cliff, without any elevation land around the centre cylinder. However, it is found from Fig. 4 (b) that, in both the X and Y profiles of the centre cone, there is elevated land around the centre cone, corresponding to the round highland.

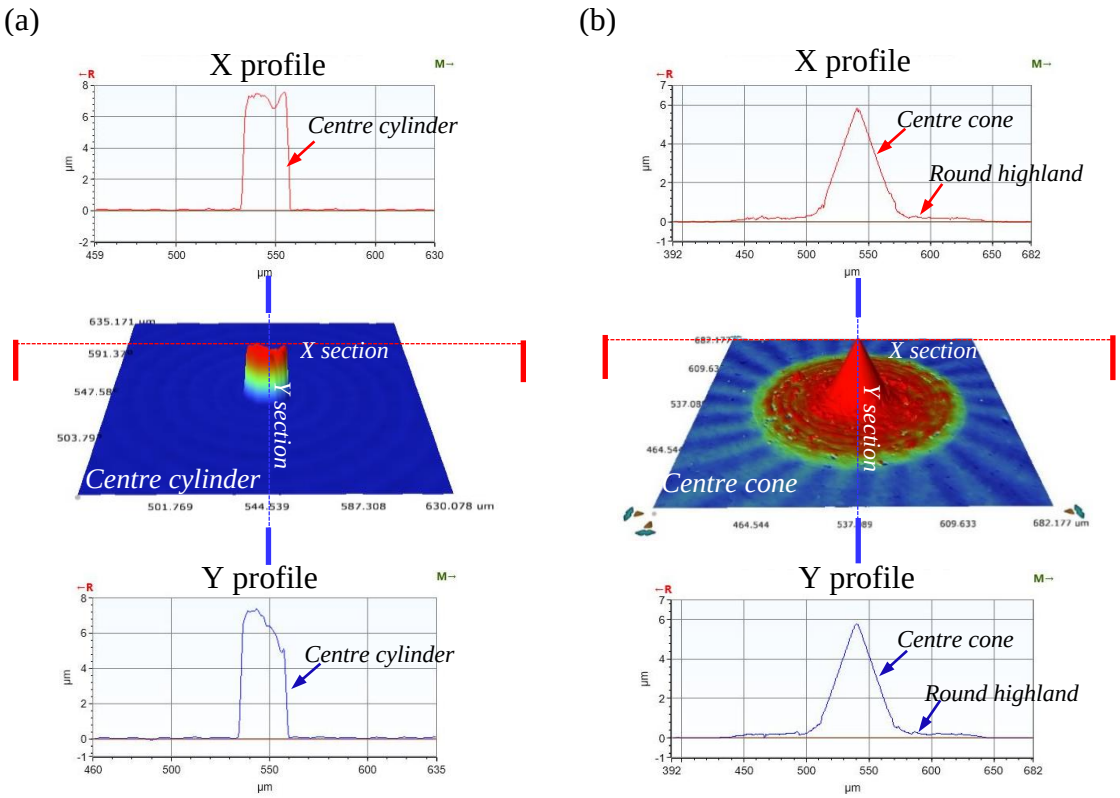

Fig.4 Comparison of centre cylinder and centre cone appearance, and its profiles in X and Y sections (cutting parameters: S_p=2000 rpm, a_p=10 μm, F_r=10 mm/min, R=0.281 mm, δ=10 °; (a) l_y=-15 μm, (b) l_y= 29.9 μm)

From the Y sectional profile of the centre cone illustrated in Fig. 5 (a), the centre cone height was measured as approximately 5.2053 μm, while the bottom radius of the centre cone is approximately 29.9 μm (bottom radius of the centre cone equals to the tool centre error l_y). Therefore, the angle between the cone generatrix and cone bottom plane can be calculated by an arctangent calculation as 9.8757. The calculated result is quite consistent with the given tool clearance angle (10 °), proving that the centre cone is formed by the tool clearance face extrusion rather than cutting. In the centre cone generation, the extrusion force elevates the cutting tool and therefore forms a round highland with a radius of 116.7 μm, which is nearly four times the size of the centre cone bottom radius, as illustrated in Fig. 5 (b). As the round highland is formed by tool interference owing to centre error, the round highland is within the tool interference zone.

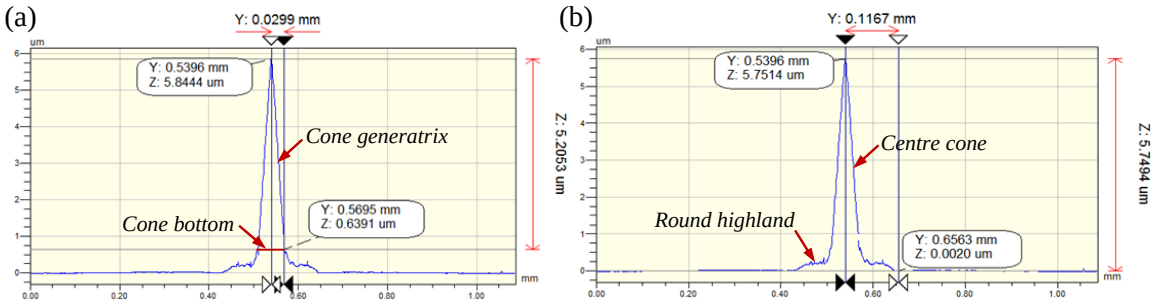

Fig. 5 (a) Sectional profile of centre cone, and (b) induced tool interference zone (cutting parameters: S_p=2000 rpm, a_p=10 μm, F_r=10 mm/min, R=0.281 mm, δ=10 °, l_y= 29.9 μm)

Figure 6 illustrates the top view and sectional profile of the tool interference zone. It is found that, from the boundary of the tool interference zone to its centre, the sectional curve can be divided into four segments, known as s_1, s_2, s_3, and s_4. Segment s_1 and s_3 are flatter, while segments s_2 and s_4 are steeper. Therefore, the diamond tool is considered to undergo two instances of elevation in both segments s_2 and s_4, which can reflect the tool interference

process and explain the rise of the cutting force at the end of the turning process. Notably, from segment s_1 to segment s_2, it is believed that a threshold, namely the tool elevation threshold, exists when the extrusion force during the centre cone formation is larger than the tool elevation threshold, where the cutting tool is elevated and a round highland is formed. However, as the extrusion force is smaller than the tool elevation threshold, although tool interference occurs, it cannot elevate the diamond tool and thus the round highland cannot be formed. Therefore, the size of the round highland is usually smaller than that of the tool interference zone.

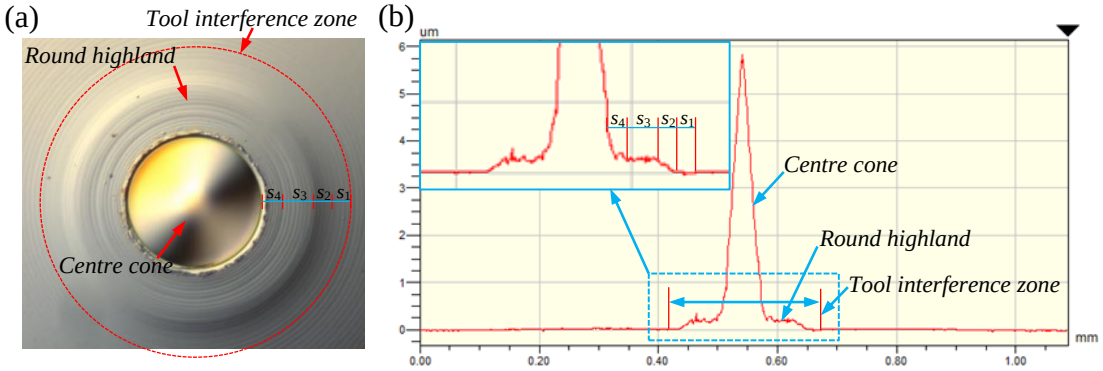

Fig. 6 (a) Tool interference zone appearance and (b) its sectional profile (S_p=2000 rpm, a_p=10 μm, F_r=10 mm/min, R=0.281 mm, δ=10 °, l_y= 29.9 μm)

3.2 Effect of process parameters on the tool interference zone

Process parameters in SPDT have some effects on the form of tool interference zone, process parameters herein include tool geometric parameters, cutting parameters and centre error. Experimental result shows that centre error, cut depth, tool nose radius and tool clearance angle have certain influence on the size and profile of tool interference zone.

Centre error is a key factor affecting the tool interference zone size. As illustrated in Fig. 7 (a), when the centre error above the spindle axis is approximately 0.0319 mm, the tool interference zone radius is approximately 0.1167 mm, and a round highland is generated. However, when the centre error above the spindle axis is approximately 0.1204 mm, as illustrated in Fig. 7 (b), the tool interference zone radius increases to 0.2506 mm, and a round highland is not observed. Therefore, the tool interference zone radius increases with an increasing centre error, and a round highland forms easily at a small centre error.

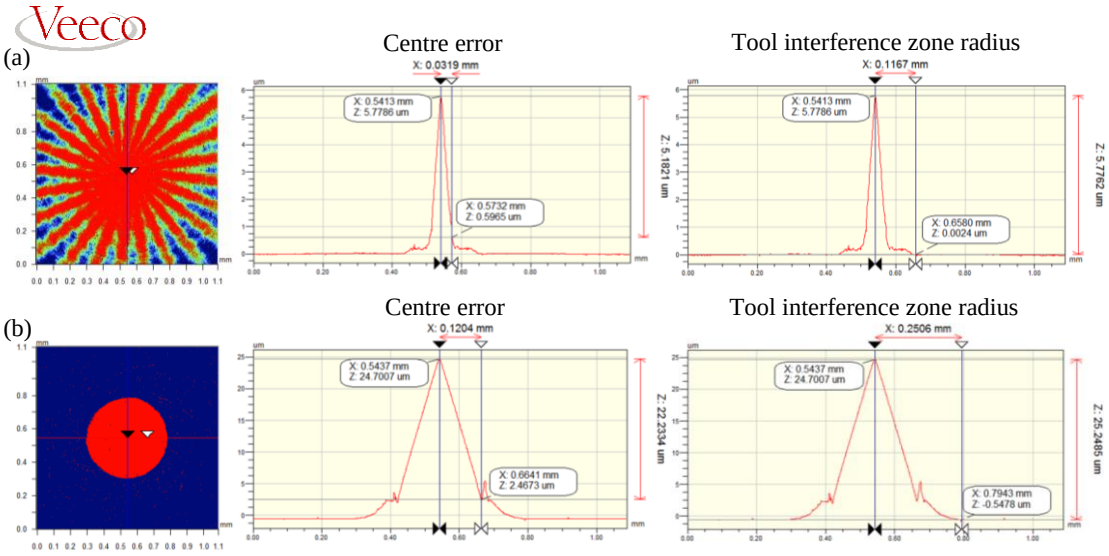

Fig. 7 Effect centre error on tool interference zone radius: (a) l_y=0.0319 mm and (b) l_y =0.1204 mm (other cutting parameters: S_p=2000 rpm, a_p=10 μm, F_r=10 mm/min, R=0.281 mm, δ=10 °)

The tool interference zone size is also affected by the cut depth. Figure 8 presents a comparison of the tool interference zone radius at different cut depths. Figure 8 (a) illustrates the centre error and its corresponding tool interference zone at a cut depth of 5 μm, while Fig. 8 (b) demonstrates these for a cut depth of 20 μm. It is found that, although SPDT exhibits the same centre error (0.1261 mm in this case), different cut depths produce varying tool interference zone radii: 0.3112 mm at a cut depth of 20 μm versus to 0.2203 mm at a cut depth of 5 μm, proving that the cut depth has a significant effect on the tool interference zone size.

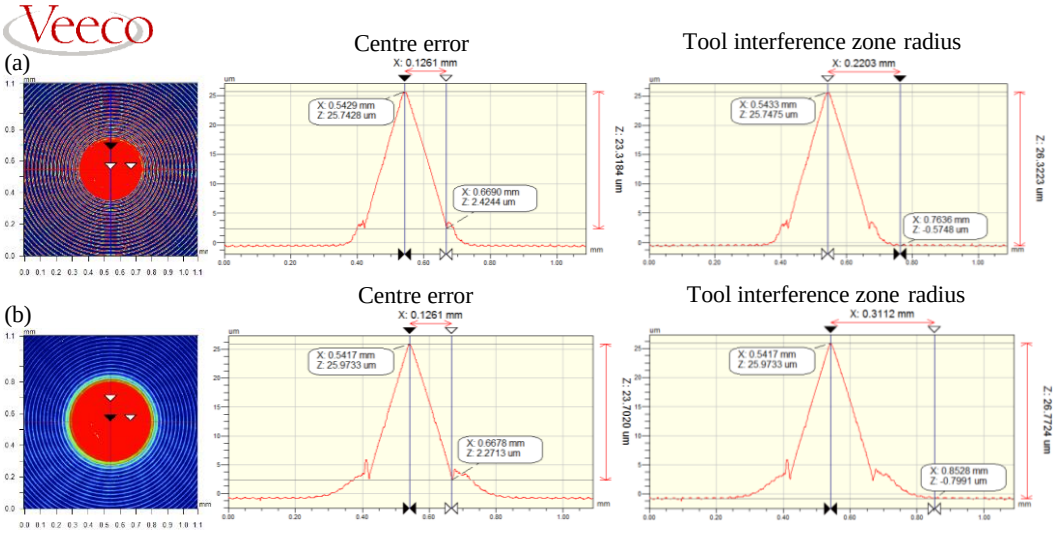

Fig. 8 Comparison of tool interference zone radius at different cut depths: (a) a_p=5 μm, (b) a_p=20 μm (other parameters: S_p=2000 rpm, F_r=10 mm/min, R=0.281 mm, δ=10 °, l_y=126.1 μm)

The tool radius is also a key factor affecting the tool interference zone size, the effects of which include two aspects: the tool nose radius affects the tool interference zone size, and the tool nose radius influences the round highland formation. Figure 9 (a) illustrates the appearance of the centre cone and its corresponding round highland at a tool nose radius of 0.101 mm, while Fig. 9 (b) depicts those at a tool nose radius of 0.514 mm. It is evident that, under nearly the same centre error (32.292 μm at a tool nose radius of 0.101 mm versus 32.175 μm at a tool nose radius of 0.514 mm), the tool interference zone radius differs substantially (79.326 μm at a tool nose radius of 0.101 mm compared to 112.326 μm at a tool nose radius of 0.514 mm), indicating that the tool nose radius has a notable effect on the tool interference zone radius. Furthermore, it is found that, compared to the tool nose radius of 0.514 mm, the tool interference zone at a tool nose radius of 0.101 mm has a round highland; therefore, it is evident that the round highland is easily formed at a small tool nose radius.

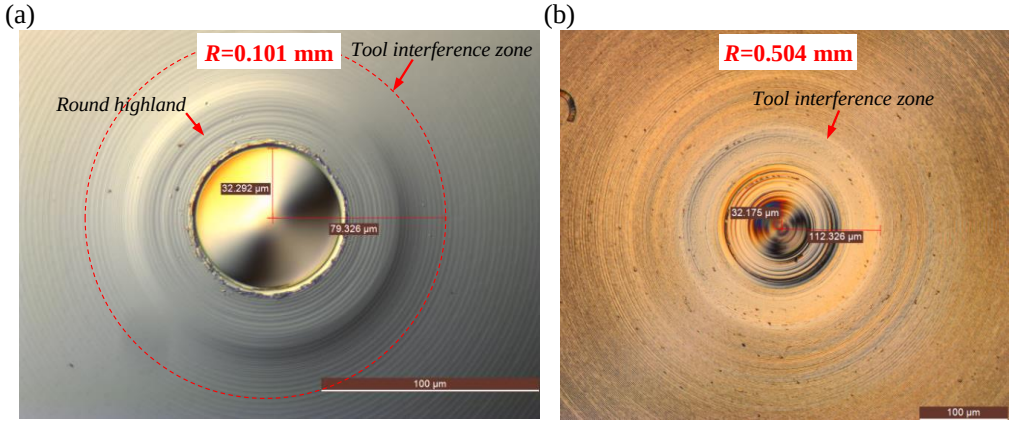

Fig. 9 Comparison of tool nose radius effects on tool interference zone radius: (a) R=0.101 mm, l_y=32.292 μm; (b) R=0.514 mm, l_y=32.175 μm (other cutting conditions: S_p=2000 rpm, a_p=8 μm, F_r=5 mm/min, δ=15 °)

Figure 10 illustrates the effects of the tool clearance angle on the tool interference zone appearance and size.

Figure 10 (a) indicates the centre error and consequent tool interference zone at a tool clearance angle of 5 °, while Fig. 10 (b) illustrates these at a tool clearance angle of 15 °. It can be observed from these two figures that, at nearly the same centre error (32.180 μm and 32.175 μm at tool clearance angles of 5 °and 15 °, respectively), the tool interference zone radius differs (142.156 μm and 112.326 μm at tool clearance angles of 5 °and 15 °, respectively); therefore, the tool interference zone radius is sensitive to the tool clearance angle. Moreover, compared to the appearance of the tool interference zone at a tool clearance angle of 15 °, a round highland is generated within the tool interference zone at a tool clearance angle of 5 °, which evidently indicates that cutting tools with a smaller tool clearance angle easily result in highland formation.

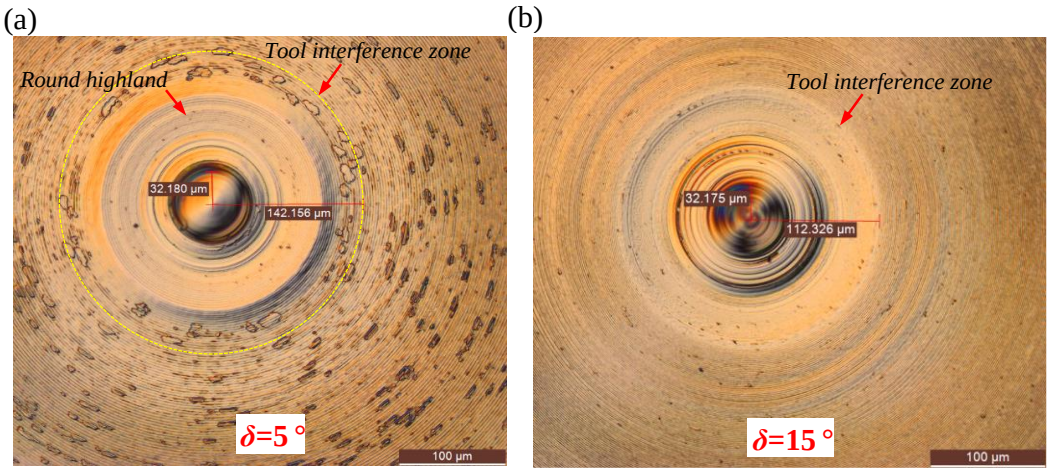

Fig. 10 Comparison of tool clearance angle effects on tool interference zone radius: (a) R=0.493 mm, l_y=32.180 μm, δ=5 °; (b) R=0.514 mm, l_y=32.175 μm, δ=15 °(other cutting conditions: S_p=2000 rpm, a_p=8 μm, F_r=5 mm/min)

From the above discussion, it can be concluded that the tool interference zone will be generated when the tool clearance extrudes to form the centre cone; however, the round highland generation depends on whether or not the extrusion force is larger than the tool elevation threshold. For different cutting conditions, the round highland may or may not be formed; however, its size must be less than that of the tool interference zone. The size of both the tool interference zone and round highland are related to the cutting conditions, which increase with an increasing centre error, cut depth and tool nose radius, but decrease with an increase in the tool clearance angle.

4. Mathematical modelling

As per the above discussion above, the centre cone is formed by the tool clearance extrusion. As the centre cone is extruded to be formed from a round platform, which is generated by the diamond tool turning. The interference between the tool clearance and round platform is a tool self-interference. During tool interference, the first contact point between the tool clearance and round platform is quite important, as it represents the tool interference zone boundary and can be used to compute the zone radius. The first contact point can be obtained by solving the common solution of the round platform tool clearance and side surface equations.

4.1 Tool interference modelling

4.1.1 Modelling of round platform side surface. In this study, commonly used cone clearance diamond tools were employed as cutting tools to perform the SPDT. During the turning process, the workpiece rotates with a certain spindle speed, while the diamond tool moves from the workpiece border to its centre, thereby producing a spiral tool path. In order to represent the turning process clearly, two coordinate systems were established: a fixed coordinate system *o-xyz* was established on the workpiece centre point, with its *x*-axis against the tool feed

direction and *z*-axis normal to the surface upwards. A moving coordinate system *o'-x'y'z'* was established on the tool tip with the same orientation as the fixed coordinate system, as illustrated in Fig. 11.

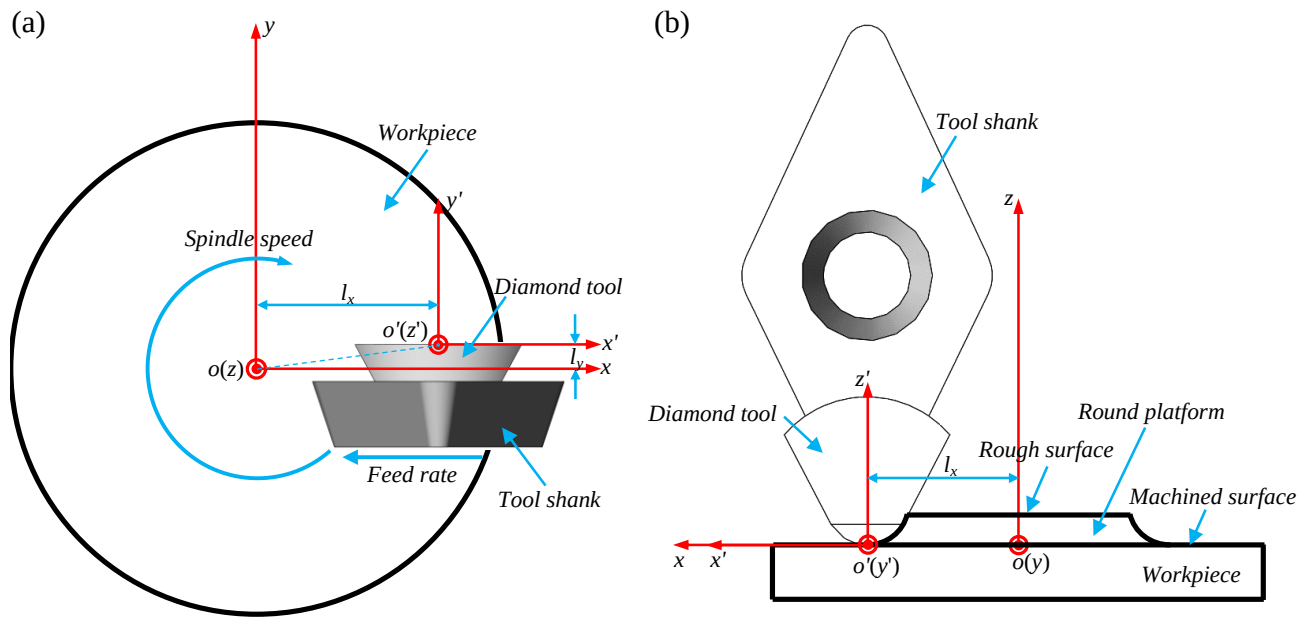

Fig. 11 Schematic of (a) tool-workpiece motion with centre error and (b) workpiece material removal process

As the cutting edge geometry is a circle, based on Fig. 11 (b), the cutting edge equation for the round platform formation can be expressed in the moving coordinate system *o'-x'y'z'* as:

$$\begin{cases} \boldsymbol{x'^2 + (z' - R)^2 = R^2} \\ \boldsymbol{y' = 0} \\ \boldsymbol{0 \le z' \le a_p} \end{cases}. \tag{1}$$

where R is the tool nose radius and a_p is the cut depth.

In Fig. 11 (a), the coordinate systems *o-xyz* and *o'-x'y'z'* have the same orientation; therefore, any point in *o'-x'y'z'* can be expressed in *o-xyz* by means of coordinate transformation:

$$\begin{bmatrix} \boldsymbol{x'} \\ \boldsymbol{y'} \\ \boldsymbol{z'} \\ \boldsymbol{1} \end{bmatrix} = \begin{bmatrix} \boldsymbol{1} & \boldsymbol{0} & \boldsymbol{0} & \boldsymbol{-l_x} \\ \boldsymbol{0} & \boldsymbol{1} & \boldsymbol{0} & \boldsymbol{-l_y} \\ \boldsymbol{0} & \boldsymbol{0} & \boldsymbol{1} & \boldsymbol{0} \\ \boldsymbol{0} & \boldsymbol{0} & \boldsymbol{0} & \boldsymbol{1} \end{bmatrix} \begin{bmatrix} \boldsymbol{x} \\ \boldsymbol{y} \\ \boldsymbol{z} \\ \boldsymbol{1} \end{bmatrix}. \tag{2}$$

where l_x is the distance between the tool centre and rotation centre in the *x*-direction, while l_y is the tool centre error above the tool feed line, as illustrated in Fig. 11.

Combining Eqs. (1) and (2), and substituting Eq. (2) for *x'*, *y'* and *z'* in Eq. (1), yields:

$$\begin{cases} \boldsymbol{(x - l_x)^2 + (z - R)^2 = R^2} \\ \boldsymbol{y = l_y} \\ \boldsymbol{0 \le z \le a_p} \end{cases}. \tag{3}$$

Equation (3) is the side surface generatrix of the round platform in coordinate system *o-xyz*.

As Eq. (3) is a curve equation in the plane of $y=l_y$, and coordinate system *o'-x'y'z'* has an offset with respect to coordinate system *o-xyz* in both the *x*- and *y*-directions, in order to form the round platform side surface, according to Fig. 11 (a), the slewing radius of each point in Eq. (3) is derived as follows:

$$\boldsymbol{s = \sqrt{x^2 + y^2} = \sqrt{x^2 + l_y^2}}. \tag{4}$$

where s is the slewing radius.

The round platform side surface can be formed by rotating the generatrix around the *z*-axis; therefore, the

equation for the round platform side surface can be obtained by combining Eqs. (3) and (4):

$$\begin{cases} \left(\sqrt{x^2+y^2-l_y{}^2}-l_x\right)^2+(z-R)^2=R^2 \\ 0\le z\le a_p \end{cases}. \tag{5}$$

4.1.2 Tool clearance face modelling. The clearance faces of diamond tools can be classified into two categories: conical and cylindrical faces, of which the diamond tool with a conical face is commonly used. In this study, a diamond tool with a conical front clearance is employed to cut the workpiece. According to the geometrical relation indicated in Fig. 12, by considering the cut depth limitation, the equation for the tool clearance face is derived as follows:

$$\begin{cases} x'^2+(z'-R)^2=\left(\frac{y'+R\cot\delta}{\cot\delta}\right)^2 \\ -\sqrt{2Ra_p-a_p{}^2}\le x'\le\sqrt{2Ra_p-a_p{}^2} \\ -a_p\cot\delta\le y'\le 0 \end{cases}. \tag{6}$$

Equation (6) is the equation for the tool clearance face with its z' coordinate in the range of (0, a_p).

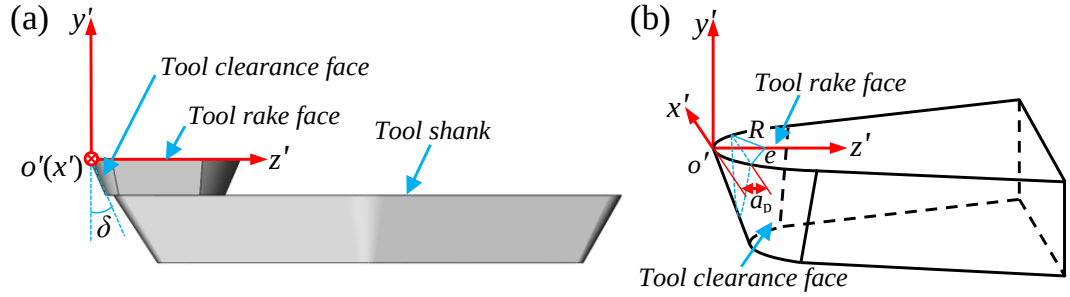

Fig. 12 Schematic of (a) conical clearance of diamond tool and (b) geometrical relation at certain cut depth

Based on the coordinate transformation of Eq. (2), Eq. (6) can be transformed into coordinate system *o-xyz*, and expressed as:

$$\begin{cases} (x-l_x)^2+(z-R)^2=\left(\frac{y-l_y+R\cot\delta}{\cot\delta}\right)^2 \\ -\sqrt{2Ra_p-a_p{}^2}+l_x\le x\le\sqrt{2Ra_p-a_p{}^2}+l_x \\ -a_p\cot\delta+l_y\le y\le l_y \end{cases}. \tag{7}$$

Equation (7) is the equation for the tool clearance face in the fixed coordinate system.

4.1.3 Modelling of tool interference zone radius. In SPDT, when the cutting tool feeds from the workpiece border to its centre, tool interference will occur at a certain point. At the position where tool interference initially occurs, not all of the cutting edges interfere simultaneously; instead, tool interference will first occur at the cutting edge with $z=a_p$, following which the interference area extends to the tool clearance face and cutting edge with a smaller z coordinate. This is because, compared to other sectional circles (c_2, c_3), the top circle (c_1) of the round platform owns the maximum curvature and z coordinate, as illustrated in Fig. 13. Therefore, at the centre error ($y=l_y$) position, the top circle of the round platform owns the maximum slope with respect to the minus of the y-axis (α_1), and

therefore tool interference occurs more easily at the top circle.

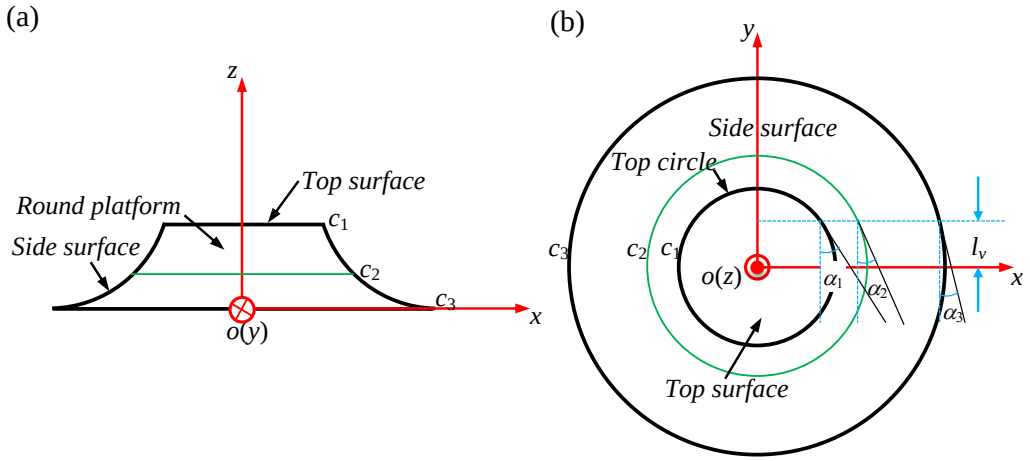

Fig. 13 Schematic of circles on round platform side surface (a) with different z coordinates, and (b) its slope at intersection point with line y=l_y

Figure 14 illustrates the virtual planes of different cut depths on a tool and their corresponding clearance intersection curves. It is found that, compared to the virtual planes with smaller cut depths (a_{p2} and a_{p3} in Fig. 14 (a)), the intersection curve between the virtual planes with a larger cut depth (a_{p1} in Fig. 14 (a)) and the tool clearance face owns a smaller slope (δ_1 in Fig. 14 (b)) at the intersection point. Therefore, tool interference occurs more easily at a greater cut depth. For both the diamond tools and round platform, tool interference first occurs at $z=a_p$; therefore, tool interference between the tool clearance face and round platform will first occur at the intersection point between the cutting edge and rough plane ($z=a_p$), following which the tool interference area extends to both the tool clearance and lower cutting edge directions. In particular, $\alpha_1=\delta_1$ is the critical condition for tool interference to take place. As δ_1 is a certain value for a cut depth provided, the occurrence of tool interference depends on α_1: tool interference occurs when α_1 is larger than δ_1; otherwise, tool interference does not occur.

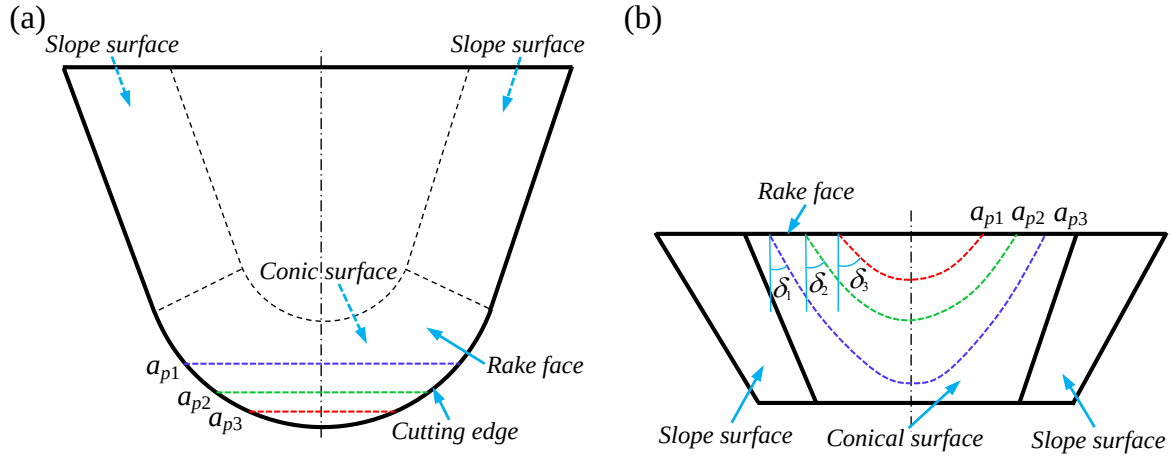

Fig. 14 Schematic of the (a) virtual planes with different cut depths on diamond tool, and (b) corresponding clearance intersection curve slopes

Refer back to Eq. (7), which indicates the equation for the tool clearance face. By defining $z = a_p$ in Eq. (6), the equation for the intersection curve between the rough surface and tool clearance face is obtained:

$$\begin{cases} x'^2 + (a_p - R)^2 = \left(\frac{y' + R\cot\delta}{\cot\delta}\right)^2 \\ -\sqrt{2Ra_p - a_p^2} \le x' \le \sqrt{2Ra_p - a_p^2} \\ -a_p\cot\delta \le y' \le 0 \end{cases} \quad (8)$$

Equation (8) is the intersection curve equation.

Defining the curve expressed by Eq. (8) and the top circle of the round platform intersecting at point *i*, according to the geometrical relation illustrated in Fig. 15, the coordinate of point *i* can be expressed in coordinate system o′-*x*′*y*′*z*′ as $(-\sqrt{2Ra_p - {a_p}^2},\ 0,\ a_p)$. Solving the derivative of *y* with respect to *x* in Eq. (9) and incorporating the coordinate of point *i* into the equation yields:

$$\boldsymbol{\cot\delta_1 = \frac{\sqrt{2Ra_p - {a_p}^2}}{R\tan\delta}.} \tag{9}$$

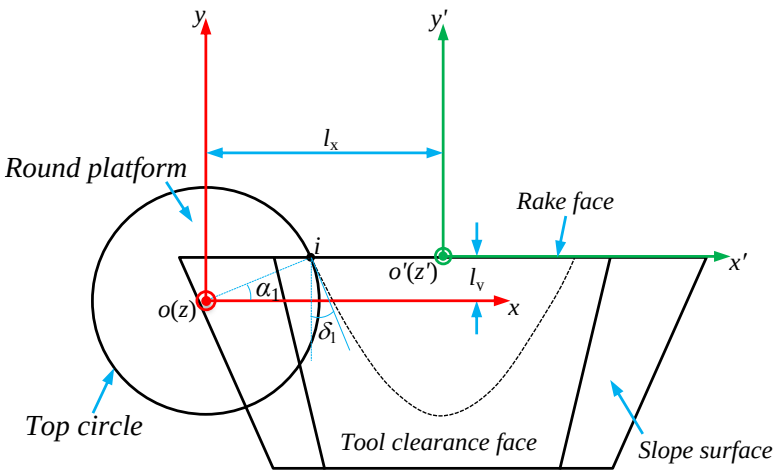

Fig. 15 Schematic of tool interference between round platform and tool clearance face

Based on Fig. 15, when tool interference first occurs, $\alpha_1=\delta_1$, and the tool interference zone radius can be obtained by:

$$\boldsymbol{r = \sqrt{{l_x}^2 + {l_y}^2}} \tag{10}$$

where l_x can be calculated by the geometrical relation, as follows:

$$\boldsymbol{l_x = l_y\cot\delta_1 + \sqrt{2Ra_p - {a_p}^2}.} \tag{11}$$

By placing Eq. (9) into Eq. (11) and then Eq. (11) into Eq. (10), the tool interference zone radius can be derived as follows:

$$\boldsymbol{r = \sqrt{\left(\frac{2Ra_p - {a_p}^2}{R\tan\delta} + 1\right)^2 {l_y}^2}.} \tag{12}$$

4.2 Relation curve of tool interference zone radius with respect to process parameters

According to Eq. (12), the tool interference zone radius is correlated with the tool nose radius, tool clearance angle, cut depth and centre error above the spindle axis. The relation curve between these is illustrated in Fig. 16, in which it can be observed that the tool interference zone radius increases with an increase in the centre error and cut depth, but decreases with an increasing tool clearance angle. Notably, with an increase in the tool nose radius, the tool interference zone radius first decreases and then increases, and therefore produces a minimum. It should be mentioned that the centre error has a significant effect on the tool interference zone radius, and their relation is close to linear.

Therefore, it can be concluded from Fig. 16 that the cutting parameters have multiple effects on the tool interference zone. Reducing the cut depth and centre error or increasing the tool clearance angle could reduce the tool interference zone and suppress the tool interference. Moreover, reducing the tool nose radius will decrease the tool interference zone radius to a certain extent.

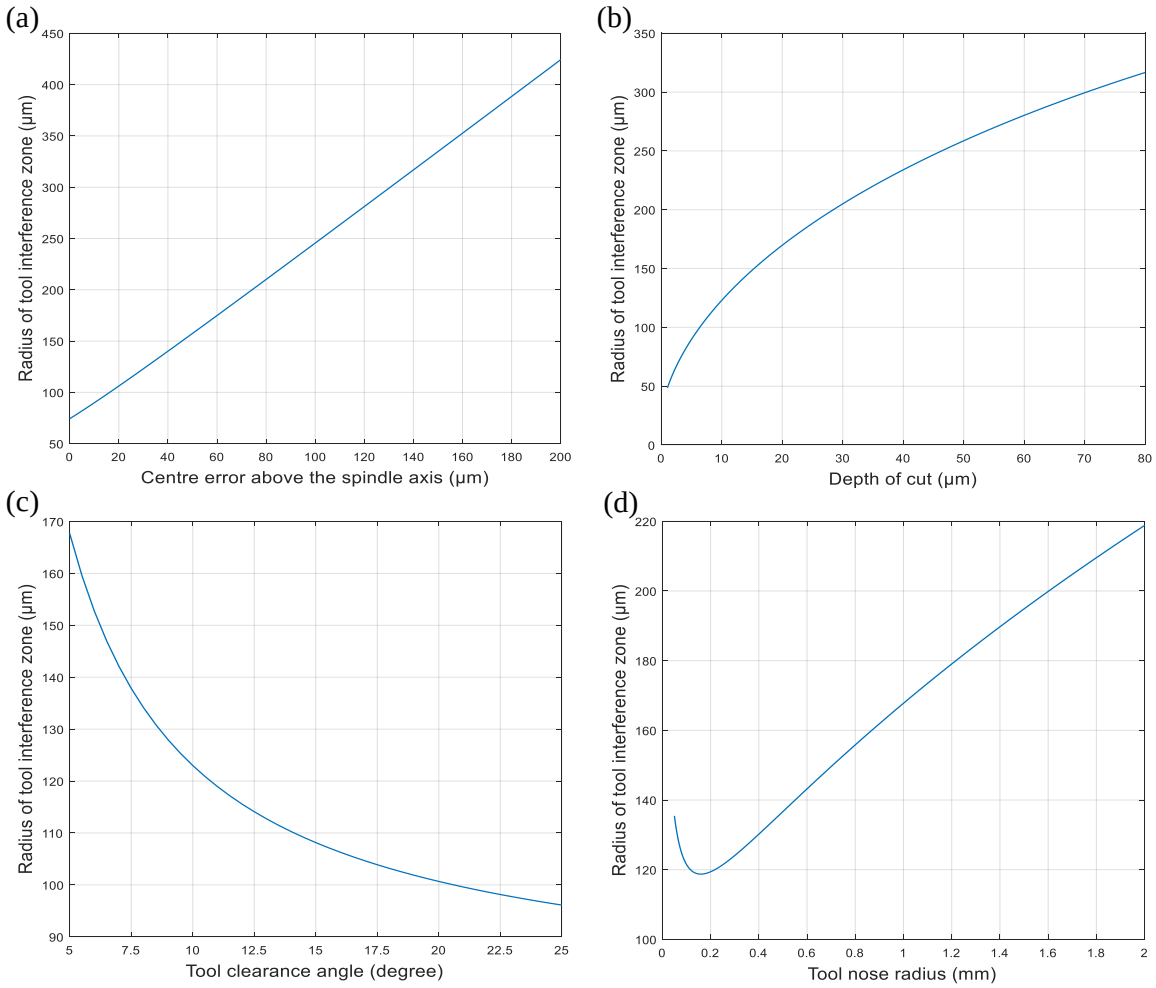

Fig. 16 Relation curves between tool interference zone radius and (a) centre error above spindle axis, (b) cut depth, (c) tool clearance angle and (d) tool nose radius

In fact, when the tool height is above the spindle axis, tool interference does occur, and the tool interference zone radius is certainly larger than $\sqrt{2\mathrm{R}a_p - {a_p}^2}$. As the cutting tool elevation owing to tool interference has a threshold, a smaller centre error may not cause obvious tool elevation; therefore, the tool interference zone may not easily be observed.

4.3 Result comparison and error analysis

Table 2 provides a comparison of the theoretical and experimental values under different tool nose radii, tool clearance angles, cut depths and centre errors. It is observed that the theoretical values are coincident to the measured values overall; however, the theoretical values are generally larger, and the maximum relative error between the values reaches 13.65%.

Table 2.

Comparison of theoretical and experimental results

Cone appearance affecting factors	Cutting parameters	Measured value (M_v)	Theoretical value (T_v)	Absolute error $\lvert M_v\text{-}T_v\rvert$	Relative error $\lvert M_v\text{-}T_v\rvert/T_v$
Tool nose radius	l_y=32 μm, a_p=8 μm, δ=15 °, R=0.101 mm	79 μm	91.7 μm	12.7 μm	13.85%
	l_y=32 μm, a_p=8 μm, δ=15 °, R=0.514 mm	112 μm	115.8 μm	3.8 μm	3.28%
Tool clearance angle	l_y=32 μm, a_p=8 μm, δ=5 °, R=0.493 mm	142 μm	157.4 μm	15.4 μm	9.69%
	l_y=32 μm, a_p=8 μm,	112 μm	115.8 μm	3.8 μm	3.28%

	δ=15 °, R=0.514 mm				
Cut depth	l_v=120 μm, a_p=5 μm, δ=10 °, R=0.281 mm	207 μm	216.8 μm	9.8 μm	4.52%
	l_v=120 μm, a_p=10 μm, δ=10 °, R=0.281 mm	251 μm	281.1 μm	30.1 μm	10.71%
Centre error	l_v=32 μm, a_p =10 μm, δ=10 °, R=0.281 mm	117 μm	124.7 μm	7.7 μm	6.17%
	l_v=120 μm, a_p =10 μm, δ=10 °, R=0.281 mm	251 μm	281.1 μm	30.1 μm	10.71%

The error sources may arise from three aspects: (1) visual error in the measurement; (2) error caused by the tool elevation threshold; and (3) error caused by the feed rate. The visual error is generated from the tool interference border distinction, which can be suppressed by repeated measurement. The tool elevation threshold also causes error when tool interference first occurs, as the top edge of the round platform is quite sharp, and the contact area between the tool clearance face and top circle of the round platform is too small to lift the diamond tool. Therefore, the tool interference zone border is difficult to distinguished, and the round highland border is mistakenly taken as the tool interference zone border. The feed rate also has a significant effect on the measurement error, particularly for a higher feed rate, as the tool path relative to the workpiece during the turning process is a helical curve, and the tool path radius varies in different directions. This can be reflected in the formation of the centre cone and corresponding tool interference zone. As illustrated in Fig. 17, the left radius of the tool interference zone is 0.1024 mm; however, the value on the right side is 0.0741 mm. Furthermore, it is found from Fig. 17 that, because of the helical tool path effect, it is difficult to measure the centre cone radius. Therefore, it is preferable to use a low feed rate to obtain a relatively accurate measurement result.

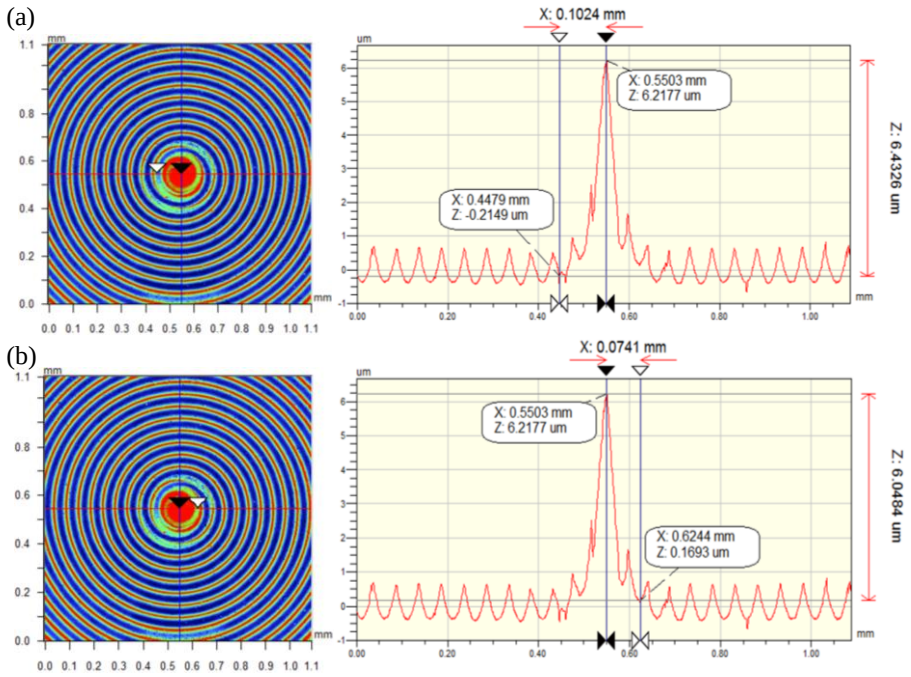

Fig. 17 Effect of feed rate on measurement of tool interference zone radius: (a) left side: r=0.1024 mm, (b) right side: r=0.0741 mm (other parameters: S_p=2000 rpm, a_p=10 μm, F_r=100 mm/min, R=0.281 mm, δ=10 °, l_y=126.1 μm)

5. Conclusion

Centre cone formation owing to centre error will result in a tool interference zone around it, seriously affecting the form accuracy of machined products. As centre error can only be reduced, rather than eliminated, it is meaningful to conduct research to explore the suppression of tool interference. In this study, theoretical and experimental research was conducted on the tool interference generation owing to centre error as well as its

influencing factors. Specific conclusions drawn from the study are as follows.

(1) The cutting force and centre error have a close relation. During centre cylinder formation, the cutting force exhibits no regular disturbance signal; however, during centre cone formation, the cutting force exhibits a force pulse, and all cutting force components in three directions approximate linear growth with the increase in centre error. This relation can potentially be used in the online identification of centre error in SPDT.

(2) A tool force pulse is formed during centre cone formation, and the workpiece centre cone is formed by extrusion of the tool clearance face, thereby elevating the diamond tool to form the tool interference zone. The tool elevation has a threshold, beyond which this diamond tool can be elevated, and forms a round highland. Therefore, the round highland is smaller than the tool interference zone and produces an error. The round highland occurs more easily at a small tool radius, centre error and tool clearance angle.

(3) A mathematical model was derived to calculate the tool interference zone radius, whereby the relation between the tool interference zone radius and cutting conditions was determined. From the mathematical model, the tool interference conditions and first tool interference position could be derived.

(4) The cutting parameters have multiple effects on the tool interference zone caused by centre error. A reduction in the cut depth and centre error and increase in the tool clearance angle could reduce the tool interference zone radius and suppress the tool interference. A reduction in the tool nose radius will first decrease the tool interference zone radius and then increase it, thereby producing a minimum. A feed rate reduction will decrease the radius difference in the tool interference zone in different directions and increase the measurement accuracy.

This research provides deep insight into the centre cone formation and resulting tool interference in SPDT, and the theoretical and experimental results can be used to suppress the centre cone occurrence. Moreover, this research provides a reference for online force-based centre error identification, thereby improving cutting efficiency.

Acknowledgement: The research proposed in this paper was supported by the National Natural Science Foundation of China (Grant No. 51505297, 51575360 and 51675347), the Natural Science Foundation of Guangdong Province (Grant No.2017A030313295), the Shenzhen Science and Technology Program (Grant No.JCYJ20160422170026058, JCYJ20160520175255386) and the Shenzhen Peacock technology innovation project(Grant No. KQJSCX20170727101318462).

References:

[1]. Evans C, Polvani R, Postek M, Rhorer R. Some observations on tool sharpness and sub-surface damage in single point diamond turning. Hague International Symposium 1987; 802:52-66.

[2]. Orra K, Choudhury S K. Mechanistic modelling for predicting cutting forces in machining considering effect of tool nose radius on chip formation and tool wear land. International Journal of Mechanical Sciences 2018; 142-143:255-268.

[3]. Namba Y, Katagiri M, Nakatsuka M. Single Point Diamond Turning of KDP Inorganic Nonlinear Optical Crystals for Laser Fusion. Journal of the Japan Society of Precision Engineering 1998; 64(10):1487-1491.

[4]. Bittner RF. Tolerancing of single point diamond turned diffractive optical elements and optical surfaces. Journal of the European Optical Society Rapid Publications 2007; 2:07028.

[5]. Zhang X, Huang R, Liu K, Kumar AS, Shan X. Rotating-tool diamond turning of Fresnel lenses on a roller mold for manufacturing of functional optical film. Precision Engineering 2018; 51:445-457.

[6]. Masuda M, Maeda Y, Nishiguchi T, Sawa M, Ikawa N. A study on diamond turning of Al–Mg alloy—generation mechanism of surface machined with worn tool. Ann. CIRP 1989; 38:111–114.

[7]. Zhang G, To S, Zhang S. Evaluation for tool flank wear and its influences on surface roughness in ultra-precision raster fly cutting. International Journal of Mechanical Sciences 2016; 118:125-134.

[8]. Lee WB, Cheung CF. A dynamic surface topography model for the prediction of nano-surface generation in ultra-precision

machining. International Journal of Mechanical Sciences 2001; 43(4):961-991.

[9]. Zong WJ, Huang YH, Zhang YL, Sun T. Conservation law of surface roughness in single point diamond turning. International Journal of Machine Tools & Manufacture 2014; 84(6): 58-63.

[10]. Iii JTC, Strenkowski JS. Finite element models of orthogonal cutting with application to single point diamond turning. International Journal of Mechanical Sciences 1988; 30(12):899-920.

[11]. Tauhiduzzaman M, Veldhuis SC. Effect of material microstructure and tool geometry on surface generation in single point diamond turning. Precision Engineering 2014; 38(3):481-491.

[12]. Juergens R C, Shepard R H, Schaefer J P. Simulation of single-point diamond turning fabrication process errors. Proceedings of SPIE - The International Society for Optical Engineering 2003; 5174.

[13]. Cheung CF, Lee WB. Surface generation in ultra-precision diamond turning: Modelling and Practices. Cromwell Press Limited, Wiltshire, UK, 2003.

[14]. Gan S W, Han-Seok L, Rahman M, Watt F. A fine tool servo system for global position error compensation for a miniature ultra-precision lathe. International Journal of Machine Tools & Manufacture 2007; 47(7):1302-1310.

[15]. Campbell A. Measurement of lathe Z-slide straightness and parallelism using a flat land. Precision Engineering 1995; 17(3):207-210.

[16]. Bryan JB. International status of thermal error research. CIRP Ann-Manuf Technol 1990; 39(2):645-656.

[17]. Liu H, Miao E, Zhuang X, Wei X. Thermal error robust modeling method for CNC machine tools based on a split unbiased estimation algorithm. Precision Engineering 2018; 51:169-175.

[18]. Mayr J, Jedrzejewski J, Uhlmann E, Donmez MA, Knapp W, Härtig F, *et al.* Thermal issues in machine tools. CIRP Annals - Manufacturing Technology 2012; 61(2):771–791.

[19]. Zhang S J, To S, Cheung C F, Wang HT. Dynamic characteristics of an aerostatic bearing spindle and its influence on surface topography in ultra-precision diamond turning. International Journal of Machine Tools & Manufacture 2012; 62(1):1-12.

[20]. Zhang S J, To S, Wang H T. A theoretical and experimental investigation into five-DOF dynamic characteristics of an aerostatic bearing spindle in ultra-precision diamond turning. International Journal of Machine Tools & Manufacture 2013; 71(8):1-10.

[21]. Tauhiduzzaman M, Yip A, Veldhuis S C. Form error in diamond turning[J]. Precision Engineering, 2015, 42:22-36.

[22]. An C, Xu Q, Zhang F, Zhang J. Calculation and structural analysis for the rigidity of air spindle in the single point diamond turning lathe. Proceedings of SPIE - The International Society for Optical Engineering 2007; 6722:67222U-67222U-8.

[23]. Wang H, To S, Chan C Y, Cheung CF, Lee WB. A theoretical and experimental investigation of the tool-tip vibration and its influence upon surface generation in single-point diamond turning. International Journal of Machine Tools & Manufacture 2010; 50(3):241-252.

[24]. Wang H, To S, Chan C Y. Investigation on the influence of tool-tip vibration on surface roughness and its representative measurement in ultra-precision diamond turning. International Journal of Machine Tools & Manufacture 2013; 69(3):20-29.

[25]. Cheung C F, Lee W B. Prediction of the Effect of Tool Interference on Surface Generation in Single-Point Diamond Turning. International Journal of Advanced Manufacturing Technology 2002; 19(4):245-252.

Figure captions：

Fig. 1 Schematic diagram of (a) centre cylinder and (b) centre cone formation

Fig. 2 (a) Experimental setup, (b) geometric parameters of diamond tools and (c) force component directions of the dynamometer (Kistler 9252A)

Fig. 3 Centre cylinder and cone appearances and corresponding cutting force forms (cutting parameters: S_p=2000 rpm, a_p=10 μm, F_r=10 mm/min, R=0.281 mm, δ=10°)

Fig.4 Comparison of centre cylinder and centre cone appearance, and its profiles in X and Y sections (cutting parameters: S_p=2000 rpm, a_p=10 μm, F_r=10 mm/min, R=0.281 mm, δ=10°; (a) l_y=-15 μm, (b) l_y= 29.9 μm)

Fig. 5 (a) Sectional profile of centre cone, and (b) induced tool interference zone (cutting parameters: S_p=2000 rpm, a_p=10 μm, F_r=10 mm/min, R=0.281 mm, δ=10°, l_y= 29.9 μm)

Fig. 6 (a) Tool interference zone appearance and (b) its sectional profile (S_p=2000 rpm, a_p=10 μm, F_r=10 mm/min, R=0.281 mm, δ=10°, l_y= 29.9 μm)

Fig. 7 Effect centre error on tool interference zone radius: (a) l_y=0.0319 mm and (b) l_y =0.1204 mm (other cutting parameters: S_p=2000 rpm, a_p=10 μm, F_r=10 mm/min, R=0.281 mm, δ=10°)

Fig. 8 Comparison of tool interference zone radius at different cut depths: (a) a_p=5 μm, (b) a_p=20 μm (other parameters*:* S_p=2000 rpm, F_r=10 mm/min, R=0.281 mm, δ=10°, l_y=126.1 μm)

Fig. 9 Comparison of tool nose radius effects on tool interference zone radius: (a) R=0.101 mm, l_y=32.292 μm; (b) R=0.514 mm, l_y=32.175 μm (other cutting conditions: S_p=2000 rpm, a_p=8 μm, F_r=5 mm/min, δ=15°)

Fig. 10 Comparison of tool clearance angle effects on tool interference zone radius: (a) R=0.493 mm, l_y=32.180 μm, δ=5°; (b) R=0.514 mm, l_y=32.175 μm, δ=15° (other cutting conditions: S_p=2000 rpm, a_p=8 μm, F_r=5 mm/min)

Fig. 11 Schematic of (a) tool-workpiece motion with centre error and (b) workpiece material removal process

Fig. 12 Schematic of (a) conical clearance of diamond tool and (b) geometrical relation at certain cut depth

Fig. 13 Schematic of circles on round platform side surface (a) with different z coordinates, and (b) its slope at intersection point with line y=l_y

Fig. 14 Schematic of the (a) virtual planes with different cut depths on diamond tool, and (b) corresponding clearance intersection curve slopes

Fig. 15 Schematic of tool interference between round platform and tool clearance face

Fig. 16 Relation curves between tool interference zone radius and (a) centre error above spindle axis, (b) cut depth, (c) tool clearance angle and (d) tool nose radius

Fig. 17 Effect of feed rate on measurement of tool interference zone radius: (a) left side: r=0.1024 mm, (b) right side: r=0.0741 mm (other parameters*:* S_p=2000 rpm, a_p=10 μm, F_r=100 mm/min, R=0.281 mm, δ=10°, l_y=126.1 μm)